Bonding of Phosphoramides onto B-C$_{59}$ Nanostructure as Drug Delivery Systems

Z. Shariatinia*

Department of Chemistry, Amirkabir University of Technology (Tehran Polytechnic), P.O. Box: 15875-4413, Tehran, Iran
(Received 11 June 2017, Accepted 3 September 2017)

The structures of boron-doped fullerene B-C$_{59}$ (1), as a drug delivery system (DDS), two phosphoramides (2 and 3), which are analogous to the cyclophosphamide anticancer prodrug, as well as their covalently bonded structures to B-C$_{59}$ (4 and 5) were optimized by DFT computations at the B3LYP level of theory using 6-31G(d) basis set. Comparing compounds 4 and 5 revealed that the chloro derivative (-1429544.59 kcal mol^{-1}) is more stable than its bromo analogue (-1429531.23 kcal mol^{-1}). The isolated drugs had almost half dipole moment values compared to those of their corresponding covalently bonded compounds with B-C$_{59}$. This reflects that the attachment of drugs to B-C$_{59}$ has considerably enhanced the polarity of the drug-carrier systems which is a desired property for drug delivery in biological media. The negative $\Delta G_{interaction}$ values for the compounds 4 and 5 confirmed that the attachment of both drugs on the surface of B-C59 has been spontaneously taken place. The negative $\Delta H_{interaction}$ values for both compounds 4 and 5 indicated that these interactions are exothermic ($\Delta H_{interaction} < 0$). The density of states (DOS) spectra disclosed that there are very strong hybridizations between the orbitals of B-C$_{59}$ and the drug molecules. The oxygen atoms of P=O and P-O bonds revealed χ values about 5.0 and 10.0 MHz, respectively that might be due to more positive oxygen atoms in P-O bonds that had a greater interaction with EFG tensor. It was established that the DDS 4 is preferred for the cancer therapy applications due to its greater $\Delta E_{binding}$, $\Delta H_{interaction}$ and $\Delta G_{interaction}$ values compared to those of DDS 5.

Keywords: B-C$_{59}$ nanocage, Phosphoramide, DFT computation, Drug delivery system, NBO

INTRODUCTION

The main methods to deliver drugs are oral and injection, which have limited the drug development. Most drugs are delivered orally or they are injected but always these are not the most suitable methods for a particular treatment [1]. For example, proteins and nucleic acids are new biological drugs which need novel delivery approaches in order to lessen side effects and to increase patient compliance [2]. Moreover, the market forces drive the need for novel and effective drug delivery methods [3]. Pharmaceutical companies can use new drug delivery methods to offer innovative drug formulations. Reformulation of old drugs can reduce side effects and increase patient compliance, consequently saving money on health care delivery [4]. Novel drug delivery systems can

utilize the drug candidates which have not been tested as trial materials [5-7]. The fullerene compounds are carbon-based, hollow, cage-like structures recognized as buckyballs as a result of their spherical structures which are similar to the geodesic domes of Buckminster Fuller. The C$_{60}$ fullerenes are familiar configurations so that the surface characteristics of these structures make them attractive for drug carrier usage.

Recently, fullerene C$_{60}$ has received much interest due to its exceptional biological activities including toxicity and antioxidant capacity [7-11]. The biological characteristics of C$_{60}$ are significantly correlated to its concentration, structure, stability and size distribution in aqueous envirinments [12]. Nevertheless, low solubility of C$_{60}$ in water suppresses its biological activities [13]. Consequently, numerous methods have been examined for the preparation of water-soluble C$_{60}$, including chemical modification [14], formation of water-soluble host–guest complexes [15,16] or

---

*Corresponding author. E-mail: shariati@aut.ac.ir

solubilization by surfactants [17,18]. The complexation of C_{60} with diverse compounds predominantly cyclodextrins [19,20], porphyrines [21], metalloporphyrines [22] and calixarenes [23,24] have been done to increase the fullerene solubility. Porphyrin adducts of cyclohexyl fullerene-C_{60} that are low toxic nanocationite particles were used to treat hypoxia prompted mitochondrial malfunction occurred in mammalian heart muscle [25]. It was found that nano-sized clusters of a teicoplanin ψ-aglycon-fullerene conjugate demonstrate antibacterial activity against enterococci resistant to teicoplanin [26].

It was established that fullerenes and their derivatives have shown numerous favourable medical applications including photosensitive oxidizing materials against malignous skin cancer [27], HIV inhibitors [28], magnetic resonance imaging (MRI) contrast compounds [29], neuroprotection by antioxidant action to heal neurodegenerative diseases [30] and gene or drug delivery vehicles [31]. Accordingly, they can be employed as drugs or carriers for different biological molecules. A number of computational approaches have often been performed on the interaction between fullerenes and different species [32]. First-principles density functional and quantum Monte Carlo calculations on light-element B and Be doped fullerenes exhibited considerably enhanced molecular H_2 binding [33].

Cyclophosphamide (CP, CAS 50-18-0) is a well-known anticancer prodrug which is activated by cytochrome P-450 in the liver [34] and shows therapeutic activity against several human cancers [35]. Literature review supports that there is not any report about the attachment of cyclophosphamide derivatives on the boron-doped fullerene surface. Thus, herein, the structural and electronic properties of compounds formed by chemical absorption of phosphoramides (which are analogues of anticancer prodrug cyclophosphamide) on the surface of boron-doped fullerene B-C_{59} (as a drug carrier) are investigated by DFT computations at B3LYP method. It was found that the DDS 4 in which phosphoramide 2 is bound to the B-C_{59} nanocage is preferred for the cancer therapy purposes due to its greater binding energy ($\Delta E_{binding}$) and thermodynamic parameters ($\Delta H_{interaction}$ and $\Delta G_{interaction}$) compared to those of DDS 5.

COMPUTATIONAL DETAILS

The structures of compounds 1-5 (Scheme 1) were first optimized in Hyperchem 7.0 program. The logP values were computed in Hyperchem to evaluate the lipophilicity of these molecules. The quantum chemical calculations were performed to fully minimize the geometries of the structures by the Gaussian 98 program [36] using density functional theory (DFT) at the B3LYP level and standard 6-31G(d) basis set. The optimizations were followed by computations of the harmonic and the vibrational frequencies, so that no imaginary frequencies were obtained at these computations. The natural bond orbital (NBO) calculations were performed to obtain the HOMO-LUMO band gap energies. The density of states (DOS) spectra were acquired using the GaussSum 2.1.6 software using the NBO output files as the input files to this software. Nuclear quadrupole coupling constants (χ) were calculated from the equation $\chi = e^2 q_{zz}Q/h$ [37], supposing that the electric quadrupole moments (Q) of ^2H, ^{17}O and ^{14}N nuclei are 2.860, -25.78 and 20.44 mb, respectively [38]. The principal components of the electric field gradient (EFG) tensor, q_{ii}, are computed in atomic unit (1 a.u. = 9.717365×10^{21} V m^{-2}), with $|q_{zz}| \geq |q_{yy}| \geq |q_{xx}|$ and $q_{xx} + q_{yy} + q_{zz} = 0$. These diagonal elements are related to each other by the asymmetry parameter: $\eta_Q = |q_{yy} - q_{xx}|/|q_{zz}|$, $0 \leq \eta_Q \leq 1$, which measures the EFG tensor deviation from axial symmetry. The computed q_{zz} component of EFG tensor is used to obtain the nuclear quadrupole coupling constants (χ).

RESULTS AND DISCUSSION

In this work, the structures of boron-doped fullerene B-C_{59} (1) and two phosphoramides (2 and 3) as well as those of their covalently bonded compounds 4 and 5 (Scheme 1) were optimized by DFT computations using B3LYP/6-31G(d) method. The binding energies for the isolated and covalently bonded drug-B-fullerene compounds were calculated from the equations $\Delta E_{binding} = E(molecule) - \Sigma_i E(atom)$. The ΔE values for the compounds 1-5 are given in Table 1. It can be observed that between compounds 2 and 3 which are only different in the halogen atoms of C-X bond (X = Cl, Br), compound 2 (chloro derivative) is more stable having a greater negative $\Delta E_{binding}$ (-3273.834 kcal mol^{-1}).
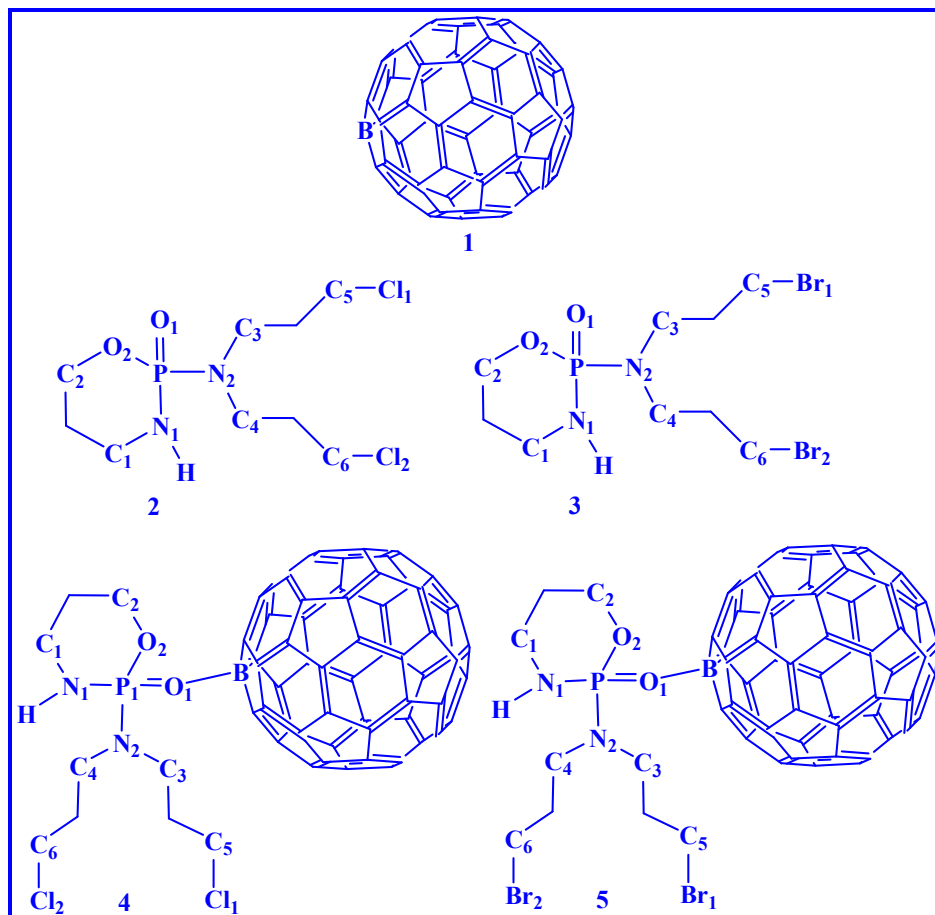
Scheme 1. The molecular structures of the compounds 1-5 indicating atom numbering.

Table 1. The Binding Energies ($\Delta E_{binding}$, kcal mol^{-1}), Dipole Moments (μ, Debye), Band Gaps ($E_g = E_{HOMO} - E_{LUMO}$, eV) and logP for the Compounds 1-5

Compound	$\Delta E_{binding}$	μ	E_g	LogP
1	-9611.96	0.5724	2.273	0.00
2	-3273.83	5.1931	2.737	3.05
3	-3259.00	5.2014	2.745	3.18
4	-1429544.59	10.518	2.037	1.64
5	-1429531.23	11.961	2.098	1.77

4   **5**
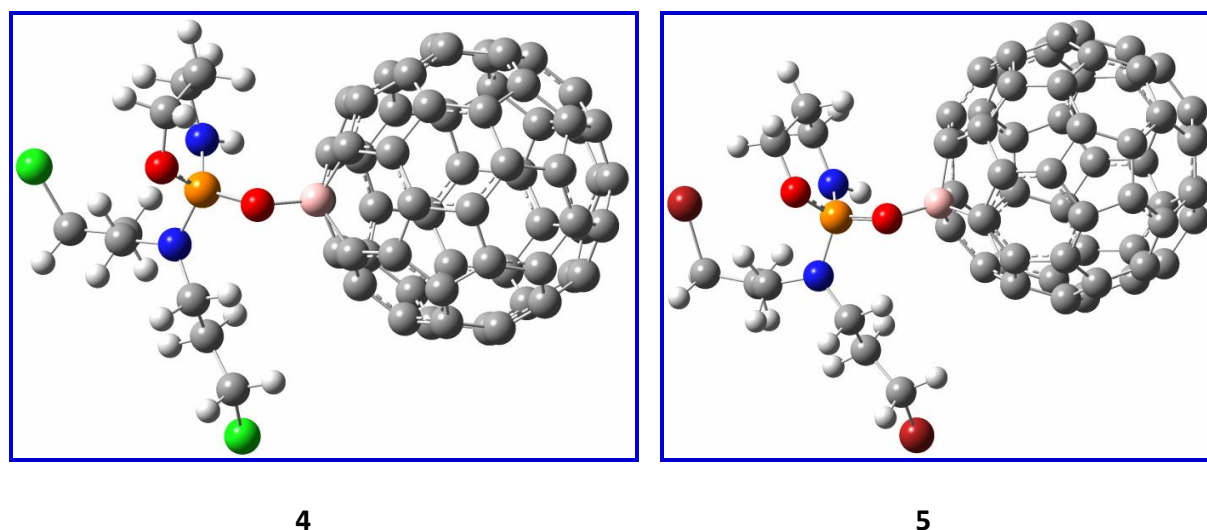
Fig. 1. The structure of compounds 4 and 5 optimized at the B3LYP/6-31G* level of theory.

Table 2. The Gibbs Free Energies ($\Delta G_{interaction}$, kcal mol^{-1}) and Enthalpies ($\Delta H_{interaction}$, kcal mol^{-1}) of Interaction for the Compounds 4 and 5

Compound	$\Delta G_{interaction}$	$\Delta H_{interaction}$
4	-9.239	-22.861
5	-9.340	-24.246

Also, comparing compounds 4 and 5 discloses that the chloro derivative (-1429544.59 kcal mol^{-1}) is slightly more stable than its bromo analogue (-1429531.23 kcal mol^{-1}).

It is observed in Table 1 that the binding energies of both compounds 4 and 5 are approximately 150 times greater than those of the B-C$_{59}$ nanocage and about 440 times higher than those of the isolated drug molecules. Therefore, it is obvious that the stability of B-C$_{59}$ nanostructure has been much highly increased after its interaction with both of the phosphoramide prodrugs. The optimized structures of the complexes 4 and 5 at B3LYP level are shown in Fig. 1 illustrating the chemical bonding of the phosphoramide prodrugs through their phosphoryl oxygen atoms onto the boron atom of B-C$_{59}$ nanocage.

The dipole moments (μ, Debye) calculated for the compounds 1-5 are shown in Table 1. The data indicate that B-C$_{59}$ has the smallest polarity with $\mu = 0.5724$ D, while compound 5 reveals the greatest μ (11.961 D). It is interesting that the dipole moments of the isolated drugs (~5.2 D) have almost half values compared with those of their related compounds covalently bonded to B-C$_{59}$ (~10.5, 12.0 D). This result illustrates that attachment of drugs on B-C$_{59}$ greatly enhances the polarity of the whole systems which is a desired property for drug delivery in biological media. It is noteworthy that the dipole moments measured for compounds formed due to physical adsorption of phosphoramides 2 and 3 on the C$_{60}$ nanocage were about 4.5 D [39] which were so much smaller than those of the

Table 3. Selected Bond Lengths (Å) and Angles (°) for the Compounds 2-5

2		3		4		5	
Bond	Bond length	Bond	Bond length	Bond	Bond length	Bond	Bond length
P-O1	1.4873	P-O1	1.4871	P-O1	1.5368	P-O1	1.5367
P-O2	1.6298	P-O2	1.6302	P-O2	1.5999	P-O2	1.5946
P-N1	1.6911	P-N1	1.6902	P-N1	1.6539	P-N1	1.6536
P-N2	1.6701	P-N2	1.6711	P-N2	1.6439	P-N2	1.6519
N1-H	1.0155	N1-H	1.0154	N1-H	1.0180	N1-H	1.0176
C5-Cl1	1.8193	C5-Br1	1.9821	C5-Cl1	1.8152	C5-Br1	1.9787
C6-Cl2	1.8180	C6-Br2	1.9811	C6-Cl2	1.8250	C6-Br2	1.9975
				O1-B	1.5882	O1-B	1.5803
Bond	Bond angle	Bond	Bond angle	Bond	Bond angle	Bond	Bond angle
O1-P-O2	114.8837	O1-P-O2	114.69	O1-P-O2	110.35	O1-P-O2	111.59
O1-P-N1	119.5517	O1-P-N1	119.72	O1-P-N1	117.15	O1-P-N1	116.06
O1-P-N2	111.2705	O1-P-N2	111.26	O1-P-N2	109.18	O1-P-N2	107.53
P-N1-H	112.4349	P-N1-H	112.46	P-N1-H	114.27	P-N1-H	114.20
				P-O1-B	128.84	P-O1-B	128.44

Table 4. Selected Wiberg Bond Orders for the Compounds 4 and 5

Bond	4	5
P-O1	1.2765	1.2787
P-O2	0.6705	0.6687
P-N1	0.7655	0.7666
P-N2	0.7617	0.7592
O2-C2	0.8727	0.8729
N1-H1	0.7932	0.7928
N1-C1	0.9670	0.9674
N2-C3	0.9518	0.9516
N2-C4	0.9599	0.9604

compounds 4 and 5 in which the drugs are chemically bonded onto the B atom of B-C_{59} nanostructure.

The band gaps (E_g) of the compounds 1-5 which their energy differences between the HOMO (highest occupied molecular orbital) and LUMO (lowest unoccupied molecular orbital) are measures of electron conductivities are presented in Table 1. It is seen that the band gaps of pristine B-C_{59} (1) and isolated drugs 2, 3 are near 2.3 and 2.7 eV, respectively while those of complexes 4, 5 are smaller (~2.0 eV) indicating decrease in electrical conductivities of the isolated drugs/B-C_{59} upon interactions. Moreover, the reduction in the band gaps verifies the interactions between the drugs and B-C_{59} nanocage.

In order to estimate the lipophilicities of compounds 1-5, their logP values were computed to predict their toxicities, Table 1. The logP values corresponding to log(1/IC_{50}) reveal that compound 5 with greater logP value (1.77) can be more toxic than 4 (logP = 1.64). It can be seen that the size of a molecule is an important parameter (steric effect) affecting the logP so that compound 5 including bigger bromo groups has a greater logP. Consequently, it can penetrate through the cell membrane more easily than 4. A comparison of the logP values achieved for DDSs 4 and 5 with those of our previously reported data for the physical adsorption of prodrugs 2 and 3 on the C_{60} nanocage illustrates that the logP values are smaller for them (1.10 and 1.23). Furthermore, the bromo derivative gave a greater logP value than its chloro analogue. This result verifies that the chemical binding of drugs improves the logP values, thus enhances the cell membrane passage by the drug-carrier systems which is very important in drug delivery purposes.

The Gibbs free energies ($\Delta G_{interaction}$) and enthalpies of interaction ($\Delta H_{interaction}$) for the compounds 4 and 5 are given in Table 2. The $\Delta G_{interaction}$ and $\Delta H_{interaction}$ are calculated using the following equations. It can be observed from Table 2 that more negative $\Delta G_{interaction}$ are obtained for the compound 5 (-9.340 kcal mol^{-1}) relative to 4 (-9.239 kcal mol^{-1}) and the attachment of both drugs on the surface of B-fullerene is exergonic ($\Delta G_{interaction} < 0$) that means these are spontaneous reactions. Similarly, the $\Delta H_{interaction}$ values are negative for both compounds 4 and 5 (-22.861 and -24.246 kcal mol^{-1}, respectively) reflecting these interactions are exothermic ($\Delta H_{interaction} < 0$).

$$\Delta G_{interaction} = G(drug\text{-}B\text{-}fullerene) - \Sigma\, G(drug) + G(B\text{-}fullerene)$$

$$\Delta H_{interaction} = H(drug\text{-}B\text{-}fullerene) - \Sigma\, H(drug) + H(B\text{-}fullerene)$$

Selected bond lengths and angles of the compounds 2-5 are listed in Table 3. The P-O1 and P-O2 bond lengths in compounds 2 and 3 are about 1.49, and 1.63 Å, while in compounds 4 and 5 they are approximately 1.54, and 1.60 Å, respectively, which are between the P-O single bond (1.64 Å) and P=O double bond (1.45 Å) lengths [40] confirming a partial multiple bond character for these P-O bonds. The smaller P-O1 bond lengths in comparison with P-O2 bond lengths display a greater bond order for the phosphoryl bond. Moreover, in complexes 4 and 5, the P-O1 bond lengths are almost 1.54 Å that are longer than those of the isolated drug molecules which is due to the attachment of drugs onto the fullerene B-C_{59} surface through their O1 atoms leading to the weakening of P-O1 bonds.

In the molecules 2 and 3, the P-N1 and P-N2 bond lengths are about 1.69, and 1.67 Å while they are near 1.65, 1.64 Å, respectively, that are close to the P-N single bond length (1.77 Å [40]). The very much slightly smaller P-N bond for the exocyclic groups may be attributed to the electron donation of halogen atoms through resonance effect leading to the more interaction of nitrogen lone pair with the phosphorus atom. Similar results were reported in the literature for the interactions of other drug-carrier systems [39,41-43]. All of the C-O and C-N bond lengths are approximately 1.44, 1.47 Å, respectively. The C-X bonds are near 1.39, 1.82 Å for X = Cl, Br, respectively, indicating smaller C-X bond for a smaller, more electronegative halogen atom. The distance measured from the phosphoryl oxygen and B atom of B-C_{59} in compounds 4 and 5 are 1.5882, 1.5803 Å, respectively, confirming a strong interaction (chemisorption) between each drug and B-C_{59} in all thermodynamically favourable compounds. It is known that the surface physical adsorption occurs by a much weaker interaction between the two compounds so that their interaction distance is longer compared with that of the chemical sorption. The equilibrium distances measured for the phosphoryl oxygen and carbon atom of fullerene C_{60} (O…C) at B3LYP level of theory in phosphoramide-C_{60}
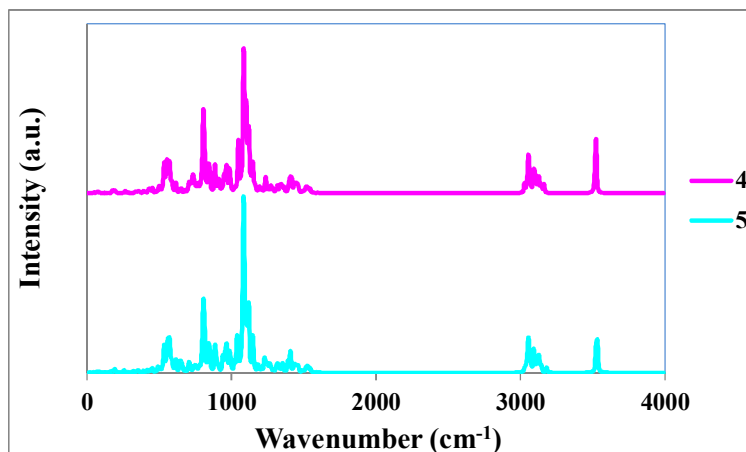
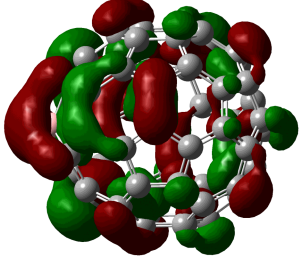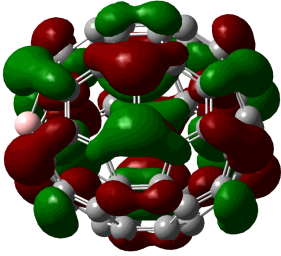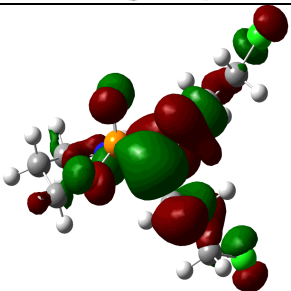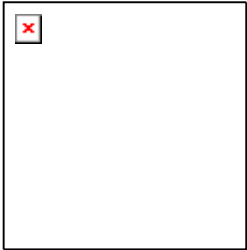**Fig. 2.** The infrared spectrum of the compound 4 obtained at the B3LYP/6-31G* level of theory.
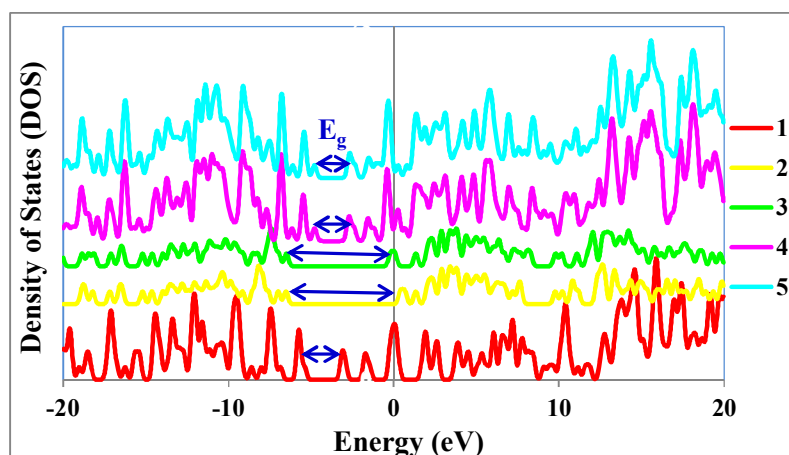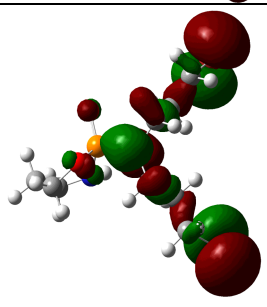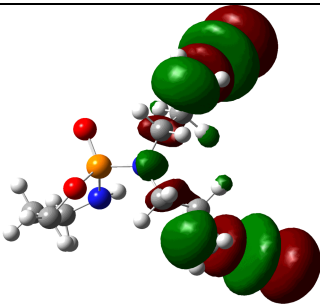
Fig. 3. The density of states (DOS) spectra of the compounds 1-5 obtained at the B3LYP/6-31G* level of theory.

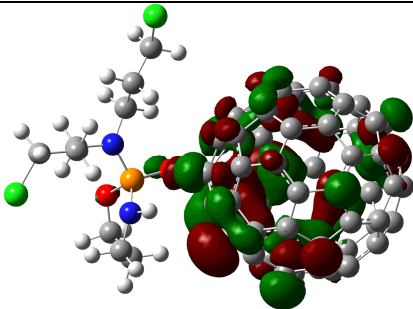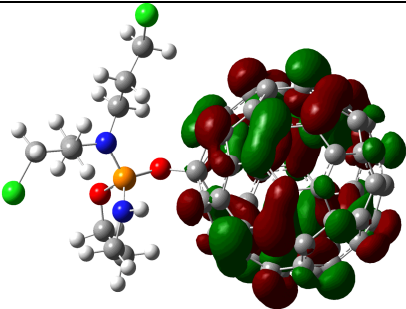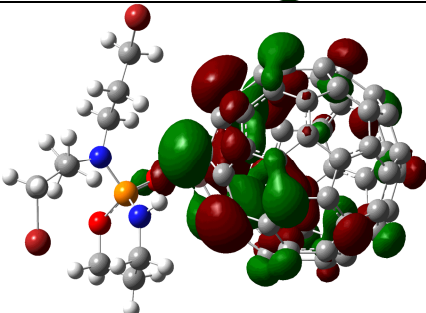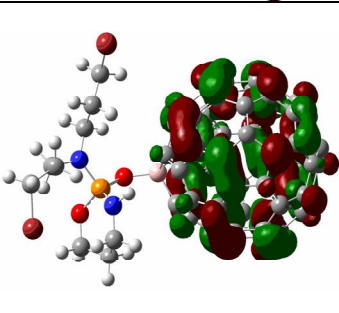complexes were near 3.3 Å reflecting a physisorption existing between drugs and C$_{60}$ carrier [39]. Therefore, the possible surface interaction mechanism between both phosphoramides 4 and 5 with B-C$_{59}$ nanostructure is a physical adsorption.

The selected Wiberg bond orders for compounds 4 and 5 are presented in Table 4 indicating that in both compounds, the bond orders of P=O and P-O are near 1.3 and 0.7, respectively. The P-N bond orders are about 0.75 but those of C-O, N-H and C-N are approximately 0.9, 0.8 and 1, respectively.

The infrared spectra of the compounds 4 and 5 are given in Fig. 2 indicating the characteristic stretching, bending and other vibrational frequencies of the CH, NH, P=O, P-O, P-N, C-C and C=C bonds in these compounds. The IR spectra exhibit stretching frequencies of O-H bonds located at around 3600-3800 cm^{-1}. The peaks near 3000 cm^{-1} are associated to the C-H stretching vibrations. The sharp peaks appeared at about 1300 cm^{-1} and 900 cm^{-1} are due to the vibrations of P=O and P-O bonds, respectively. The bands existing at around 1000 cm^{-1} can be assigned to the stretching frequencies of C-C bonds and the bands at about 1350, 1400 cm^{-1} are related to the asymmetric and symmetric bending deformations of CH$_2$/CH$_3$ bonds. The

Compound	HOMO	LUMO
1		
2		
3		
4		
5		

Fig. 4. The HOMOs and LUMOs of the compounds 1-5
(red and green colors represent negative and positive regions of the wave functions, respectively).

Compound	ESP	Contour map
1		
2		
3		
4		
5		
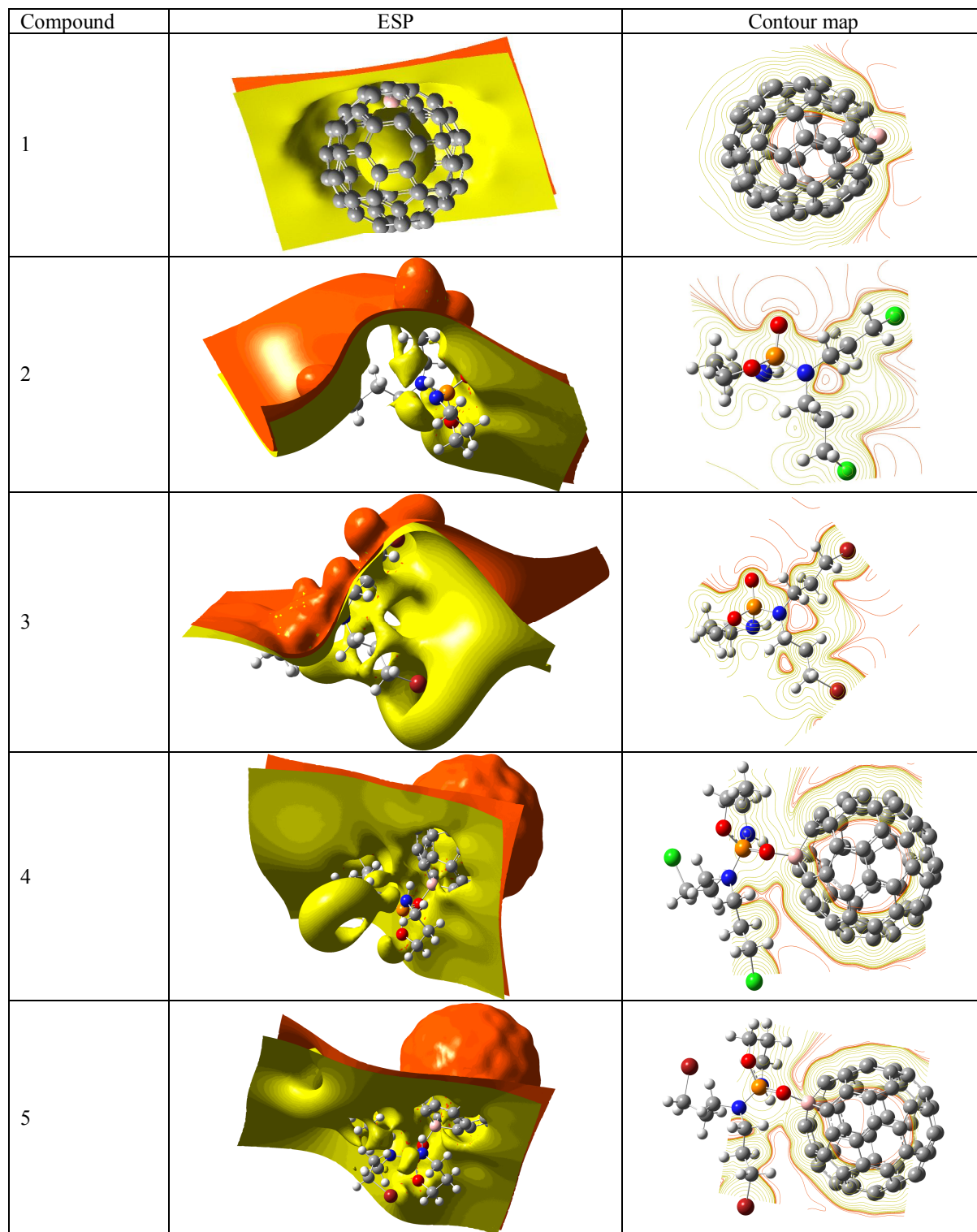
Fig. 5. The electrostatic surface potentials (ESPs) and contour maps for the compounds 1-5. (red and yellow colors represent negative and positive regions of the wave functions, respectively).

Table 5. Calculated Nuclear Quadrupole Coupling Constants (χ) for ^{2}H (kHz) and ^{17}O, ^{14}N, ^{35}Cl (MHz) Nuclei of 2-5

2		3		4		5	
Nucleus	χ	Nucleus	χ	Nucleus	χ	Nucleus	χ
O1	4.9461	O1	4.9460	O1	7.0870	O1	7.1575
O2	9.7377	O2	9.7482	O2	9.3545	O2	9.5618
N1	4.8877	N1	4.8996	N1	4.8246	N1	4.9672
N2	5.4713	N2	5.4409	N2	5.1403	N2	5.3204
H1	254.71	H1	254.84	H1	238.53	H1	240.95
^{35}Cl1	69.764	^{79}Br1	495.96	^{35}Cl1	68.441	^{79}Br1	469.46
^{35}Cl2	69.435	^{79}Br2	493.17	^{35}Cl2	70.378	^{79}Br2	499.69
^{37}Cl1	54.982	^{81}Br1	415.15	^{37}Cl1	53.939	^{81}Br1	392.97
^{37}Cl2	54.723	^{81}Br2	412.82	^{37}Cl2	55.465	^{81}Br2	418.27

bands observed near 700 cm^{-1} may be attributed to the rocking vibrations of CH$_2$/CH$_3$ bonds. The peaks detected at approximately 3200-3300 cm^{-1} are allocated to the stretching frequencies of NH bonds.

To further interpret the nature of the binding in these systems, the electronic structures of compounds 4 and 5 were studied. For this purpose, their density of states (DOS) spectra were calculated and indicated in Fig. 3. It is evidently observed that there are very strong hybridizations between the orbitals of B-C$_{59}$ (1) and the drug molecules (2 and 3) so that the DOS spectra illustrate combinations of the spectra of both drugs and B-C$_{59}$. As a result, great interactions occurs quantitatively in terms of binding energies. This can be deduced from the occurrence of very different DOS spectral patterns for the compounds 4 and 5 compared with their corresponding isolated constituents including B-C$_{59}$ and drug molecules. The DOS spectra also display the changes in band gaps of the drugs before and after their binding onto the B-C$_{59}$ nanocage. It is obviously seen that the energy gaps of drugs are decreased after their attachment onto the B-C$_{59}$ carrier. Similar results were reported in the literature for the interactions of other drug-carrier systems [39,41,42].

The frontier molecular orbitals of the compounds 1-5 are shown in Fig. 4 in which the red and green colors represent negative and positive regions of the wave functions, respectively. It is observed that the HOMO is almost symmetrically dispersed on the B-C$_{59}$ nanocage with a greater accumulation of orbitals on the B atom but the dispersion of the LUMO on the B-C$_{59}$ is totally symmetric. The HOMO in prodrug 2 is nearly positioned on the entire parts of the molecule except for some carbon and hydrogen atoms of the CH$_2$ groups while the LUMO is mostly distributed on the (CH$_2$)$_2$Cl moieties of the N[(CH$_2$)$_3$Cl]$_2$ group. In phosphoramide compound 3, the HOMO is mainly located on the atoms of N[(CH$_2$)$_3$Cl]$_2$ group but the location of its LUMO is similar to that of the compound 2 that is primarily placed on the (CH$_2$)$_2$Cl moieties of the N[(CH$_2$)$_3$Cl]$_2$ group. In drug delivery systems 4 and 5, both of the HOMO and LUMO are practically observed on the B-C$_{59}$ nanocage.

The distribution of electron density of a molecule is presented using both electrostatic surface potentials (ESPs) and contour maps. The contour maps and ESPs for the compounds 1-5 are exhibited in Fig. 4. In these images, red and yellow colors represent negative and positive regions of

the wave functions, respectively. The existence of B atom in the B-C$_{59}$ nanocage has changed the totally symmetric distribution of negative charges leading to accumulation of negative charges toward the B atom which is obviously observed in the ESP and contour map. In phosphoramide prodrugs, the charge distributions are unsymmetric and negative charges are mostly distributed on the oxygen, chloride and nitrogen atoms which result in very unsymmetric ESP and contour map images. It is observed that attachment of the two prodrugs on the B-C$_{59}$ nanocage alters the charge distribution of the drug delivery systems 4 and 5 so that the negative charges are primarily placed on the B-C$_{59}$ nanostructure and some atoms of drugs which are close to B-C$_{59}$ and nothing is observed on the other atoms of drugs that are far from the nanocage. Furthermore, it is found that the charge distribution is the highest asymmetric for the compounds 4 and 5 but it is the lowest asymmetric for the prodrugs 2 and 3 leading to the greatest dipole moment for 4 and 5 (~5.1 D) while the smallest dipole moment for the 2 and 3 (~11.0 D), see Table 1. Similar to the contour maps, the ESP images reveal the distributions of the electric charges exhibiting their high polarity. After binding the drugs onto the B-C$_{59}$, asymmetry in the electric charge is visualized that is in agreement with the dipole moments data (Table 1).

Selected calculated nuclear quadrupole coupling constants (χ) for the quadrupole ^{14}N, ^{2}H, ^{17}O, ^{35}Cl, ^{37}Cl, ^{79}Br and ^{81}Br nuclei of the compounds 2-5 are presented in Table 5. In all compounds, the exocyclic nitrogen atoms indicate χ values greater than those of endocyclic N atoms within the aliphatic six-membered ring. This may be attributed to the more positive charge that exists on the exocyclic nitrogen leading to its stronger interaction with the electric field gradient. Furthermore, the oxygen atoms of P=O and P-O bonds reveal χ values about 5.0 and 10.0 MHz, respectively. The reason for the almost half χ values of oxygen atoms in phosphoryl moieties relative to those of P-O groups could be more positive oxygen atoms in P-O bonds that have a greater interaction with EFG tensor. Interestingly, the phosphoryl O atoms of the compounds 4 and 5 show greater NQCCs compared with those of the isolated drugs confirming that the O1 environment has become more asymmetric upon its attachment to the B atom of B-C$_{59}$ nanocage. The χ values for ^{14}N and ^{2}H atoms are about 5

MHz and 255 KHz, respectively. Comparable results were obtained for some previously studied phosphoramides [39,43]. The ^{35}Cl and ^{37}Cl nuclei demonstrate NQCCs of about 70 and 55 MHz, respectively. The ^{79}Br and ^{81}Br nuclei reveal NQCCs of about 500 and 420 MHz, respectively.

In order to make a comparison between our results with those of the experimentally reported published papers using fullerene derivatives as drug carriers, it should be mentioned that C$_{60}$ family have been widely applied for drug delivery purposes and have shown desirable performance. For instance, C$_{60}$ fullerene-doxorubicin complex was employed for tumor cell treatment both *in vitro* and *in vivo* [44]. Also, fullerenol C$_{60}$(OH)$_{24}$ exhibited cytotoxicity induced by antitumor drugs on human breast carcinoma cell lines [45]. In another work, the PEGylated fullerene-5-fluorouracil conjugates were synthesized and utilized to enhance the antitumor influence of 5-fluorouracil [46]. Recently, C$_{60}$ was used as an efficient carrier for the delivery of methotrexate to breast cancer cells [47]. The docetaxel was delivered while employing glycine-tethered C$_{60}$-fullerenes and displayed enhanced cellular uptake, improved efficacy and favourable pharmacokinetic profile [48]. Moreover, appropriate results were achieved for the biotransportation and biodistribution of fluorescent [60] fullerene in a murine orthotopic model of breast adenocarcinoma using the non-invasive radiofrequency electric field hyperthermia [49]. Thus, it may be suggested that our DDSs 4 and 5 (and especially 4) have promising potential to be used as anticancer vehicles.

CONCLUSIONS

The covalent bonding of anticancer phosphoramides (2 and 3) through the phosphoryl oxygen atom to the B-C$_{59}$ surface was investigated by DFT computations using the B3LYP/6-31G(d) approach. The binding energy values illustrated that between the compounds 2 and 3 that their only difference is in the halogen atoms of C-X bond (X = Cl, Br), compound 2 is more stable having a greater negative $\Delta E_{binding}$ (-3273.83 kcal mol^{-1}). Also, comparing compounds 4 and 5 showed that the chloro derivative (-1429544.59 kcal mol^{-1}) is somewhat more stable than its bromo analogue (-1429531.23 kcal mol^{-1}). In the molecules

2 and 3, the P-N1 and P-N2 bond lengths were near 1.69, 1.67 Å but they were near 1.65, 1.64 Å, respectively, that are close to the P-N single bond length (1.77 Å). All of the Gibbs free energies ($\Delta G_{interaction}$) and enthalpies of the interaction ($\Delta H_{interaction}$) for the compounds 4 and 5 were negative confirming the interactions were both exergonic and exothermic. The logP values disclosed that the compound 5 with greater logP value (1.77) could be more toxic than 4 (logP = 1.64) suggesting that the size of a molecule is a significant parameter (steric effect) affecting logP so that the compound 5 including bigger bromo groups had a greater logP. Consequently, it could penetrate through the cell membrane more easily than 4. In drug delivery systems 4 and 5, both of the HOMO and LUMO were practically observed on the B-C_{59} nanocage. In all compounds, the exocyclic nitrogen atoms indicated χ values greater than those of endocyclic N atoms within the aliphatic six-membered ring. The ^{35}Cl, ^{37}Cl and ^{79}Br, ^{81}Br nuclei demonstrated NQCCs of about 70, 55 and 500, 420 MHz, respectively. It was shown that the drug delivery system 4 is more suitable compared to 5 for cancer therapy applications because of its greater $\Delta E_{binding}$ and $\Delta H_{interaction}$ and $\Delta G_{interaction}$ values.

ACKNOWLEDGMENTS

REFERENCES

[1]   Bradbury, J., Beyond pills and jabs. *Lancet,* **2003**, *362* (9400), 1984-1985, DOI: 10.1016/S0140-6736(03)15086-6.

[2]   Kefalides, P. T., New methods for drug delivery. *Ann. Intern. Med.,* **1998**, *128* (12_Part_1), 1053-1055, DOI: 10.7326/0003-4819-128-12_Part_1-199806150-00039.

[3]   VisionGain, Drug delivery 2003: new technologies in the global market. VisionGain, June 2003.

[4]   Henry, C. M., New wrinkles in drug delivery. *Chem. Eng. News,* **2004**, *82*, 37-42, DOI:10.1021/cen-v082n009.p037.

[5]   Emerich, D. F.; Thanos, C. G., The pinpoint promise of nanoparticle-based drug delivery and molecular diagnosis. *Biomol. Eng.,* **2006**, *23*, 171-184, DOI: 10.1016/j.bioeng.2006.05.026.

[6]   Fischer, H. C.; Chan, W. C. W., Nanotoxicity: the growing need for *in vivo* study. *Curr. Opin. Biotechnol.,* **2007**, *18*, 565-571, DOI: 10.1016/j.copbio.2007.11.008.

[7]   Faraji, A. H.; Wipf, P., Nanoparticles in cellular drug delivery. *Bioorg. Med. Chem.,* **2009**, *17*, 2950-2962, DOI: 10.1016/j.bmc.2009.02.043.

[8]   Sayes, C. M.; Marchione, A. A.; Reed, K. L.; Warheit, D. B., Comparative pulmonary toxicity assessments of C60 water suspensions in rats: few differences in fullerene toxicity in vivo in contrast to *in vitro* profiles. *Nano Lett.,* **2007**, *7*, 2399-2406, DOI: 10.1021/nl0710710.

[9]   Markovic, Z.; Trajkovic, V., Biomedical potential of the reactive oxygen species generation and quenching by fullerenes (C60). *Biomaterials,* **2008**, *29*, 3561-3573, DOI: 10.1016/j.biomaterials.2008.05.005.

[10]   Song, M. Y.; Jiang, G. B.; Yin, J. F.; Wang, H. L., Inhibition of polymerase activity by pristine fullerene nanoparticles can be mitigated by abundant proteins. *Chem. Commun.,* **2010**, *46*, 1404-1406, DOI: 10.1039/B922711C.

[11]   Trpkovic, A.; Todorovic-Markovic, B.; Trajkovic, V., Toxicity of pristine versus functionalized fullerenes: mechanisms of cell damage and the role of oxidative stress. *Arch. Toxicol.,* **2012**, *86*, 1809-1827, DOI: 10.1007/s00204-012-0859-6.

[12]   Deguchi, S.; Alargova, R. G.; Tsujii, K., Stable dispersions of fullerenes, C60 and C70, in water. preparation and characterization. *Langmuir,* **2001**, *17,* 6013-6017, DOI: 10.1021/la010651o.

[13]   Liu, Y.; Wang, H.; Liang, P.; Zhang, H. Y., Water-soluble supramolecular fullerene assembly mediated by metallobridged β-cyclodextrins. *Angew. Chem. Int. Ed.,* **2004**, *43*, 2690-2694, DOI: 10.1002/anie.200352973.

[14]   Tokuyama, H.; Yamago, S.; Nakamura, E.; Shiraki, T.; Sugiura, Y., Photoinduced biochemical activity of fullerene carboxylic acid. *J. Am. Chem. Soc.,* **1993**, *115*, 7918-7919, DOI: 10.1021/ja00070a064.

[15] Ikeda, A.; Yoshimura, M.; Shinkai S., Solution complexes formed from C60 and calixarenes. On the importance of the preorganized structure for cooperative interactions. *Tetrahedron Lett.,* **1997**, *38*, 2107-2110, DOI: 10.1016/S0040-4039(97)00318-3.

[16] Cao, R.; Wu, S., In silico properties characterization of water-soluble γ-cyclodextrin bi-capped C60 complex: Free energy and geometrical insights for stability and solubility. *Carbohydr. Polym.,* **2015**, *124*, 188-195, DOI: 10.1016/j.carbpol.2015.02.014.

[17] Xiao, L.; Takada, H.; Gan Xue, H.; Miwa, N., The water-soluble fullerene derivative 'Radical Sponge®' exerts cytoprotective action against UVA irradiation but not visible-light-catalyzed cytotoxicity in human skin keratinocytes. *Bioorg. Med. Chem. Lett.,* **2006**, *16*, 1590-1595, DOI: 10.1016/j.bmcl.2005.12.011.

[18] Iwamoto, Y.; Yamakoshi, Y., A highly water-soluble C60–NVP copolymer: a potential material for photodynamic therapy. *Chem. Commun.,* **2006**, *46*, 4805-4807, DOI: 10.1039/B614305A.

[19] Yoshida, Z.; Takekuma, H.; Takekuma, S.; Matsubara, Y., Molecular recognition of C60 with γ-cyclodextrin. *Angew. Chem. Int. Ed. Engl.,* **1994**, *33*, 1597-1599, DOI:10.1002/anie.199415971.

[20] Andersson, T.; Nilsson, K.; Sundahl, M.; Westman, G.; Wennerstroem, O., C60 embedded in γ-cyclodextrin: a water-soluble fullerene. *J. Chem. Soc. Chem. Commun.,* **1992**, *8*, 604-606, DOI: 10.1039/C39920000604.

[21] Rezayat, S. M.; Boushehri, S. V. S.; Salmanian, B.; Omidvari, A. H.; Tarighat, S.; Esmaeili, S.; Sarkar, S.; Amirshahi, N.; Alyautdin, R. N.; Orlova, M. A.; Trushkov, I. V.; Buchachenko, A. L.; Liu, K. C.; Kuznetsov, D. A., The porphyrin-fullerene nanoparticles to promote the ATP overproduction in myocardium: 25Mg^{2+} magnetic isotope effect. *Eur. J. Med. Chem.,* **2009**, *44*, 1554-1569, DOI: 10.1016/j.ejmech.2008.07.030.

[22] Konareva, D. V.; Khasanov, S. S.; Lyubovskaya, R. N., Fullerene complexes with coordination assemblies of metalloporphyrins and metal phthalocyanines. *Coord. Chem. Rev.,* **2014**, *262*, 16-36, DOI: 10.1016/j.ccr.2013.10.021.

[23] Dumitriu, C.; Mousavi, Z.; Latonen, R. -M.; Bobacka, J.; Demetrescu, I., Electrochemical synthesis and characterization of poly(3,4-ethylenedioxythiophene) doped with sulfonated calixarenes and sulfonated calixarene-fullerene complexes. *Electrochim. Acta,* **2013**, *107*, 178-186, DOI: 10.1016/j.electacta.2013.05.140.

[24] Mizyed, S. A.; Al-Jarrah, E.; Marji, D.; Ashram, M., A spectrophotometric study of the charge transfer complexes of [60] fullerene with different tert-butylcalix[4]crowns. *Spectrochim. Acta Part A,* **2007**, *68*, 1274-1277, DOI:10.1016/j.saa.2007.02.004.

[25] Amirshahi, N.; Alyautdin, R. N.; Sarkar, S.; Rezayat, S. M.; Orlova, M. A.; Trushkov, I. V.; Buchachenko, A. L.; Kuznetsov, D. A., Fullerene-based low toxic nanocationite particles (porphyrin adducts of cyclohexyl fullerene-C60) to treat hypoxia-induced mitochondrial dysfunction in mammalian heart muscle. *Arch. Med. Res.,* **2008**, *39*, 549-559, DOI: 10.1016/j.arcmed.2008.05.007.

[26] Tollas, S.; Bereczki, I.; Sipos, A.; Rőth, E.; Batta, G.; Daróczi, L.; Kéki, S.; Ostorházi, E.; Rozgonyi, F.; Herczegh, P., Nano-sized clusters of a teicoplanin ψ-aglycon-fullerene conjugate. Synthesis, antibacterial activity and aggregation studies. *Eur. J. Med. Chem.,* **2012**, *54*, 943-948, DOI: 10.1016/j.ejmech.2012.06.054.

[27] DeRosa, M. C.; Crutchley, R. J., Photosensitized singlet oxygen and its applications. *Coord. Chem. Rev.,* **2002**, *233-234*, 351-371, DOI: 10.1016/S0010-8545(02)00034-6.

[28] Friedman, S. H.; DeCamp, D. L.; Sijbesma, R. P.; Srdanov, G.; Wudl, F.; Kenyon, G. L., Inhibition of the HIV-1 protease by fullerene derivatives: model building studies and experimental verification. *J. Am. Chem. Soc.,* **1993**, *115*, 6506-6509, DOI: 10.1021/ja00068a005.

[29] Cagle, D. W.; Kennel, S. J.; Mirzadeh, S.; Alford, J. M.; Wilson, L. J., *In vivo* studies of fullerene-based materials using endohedral metallofullerene radiotracers. *Proc. Natl. Acad. Sci. USA,* **1999**, *96*, 5182-5187, DOI:10.1073/pnas.96.9.5182.

[30] Dugan, L. L.; Turetsky, D. M.; Du, C.; Lobner, D.; Wheeler, M.; Almli, C. R.; Shen, C. K. F.; Luh, T. -Y.; Choi, D. W.; Lin, T. -S., Carboxyfullerenes as

neuroprotective agents. *Proc. Natl. Acad. Sci. USA,* **1997**, *94*, 9434-9439.

[31] Montellano, A.; Da Ros, T.; Bianco, A.; Prato, M., Fullerene C60 as a multifunctional system for drug and gene delivery. *Nanoscale,* **2011**, *3*, 4035-4041, DOI: 10.1039/C1NR10783F.

[32] Tachikawa, H.; Iyama, T.; Abe, S. DFT study on the interaction of Fullerene (C60) with hydroxyl radical (OH). *Phys. Procedia,* **2011**, *14*, 139-142, DOI: 10.1016/j.phpro.2011.05.027.

[33] Kim, Y. -H.; Zhao, Y.; Williamson, A.; Heben, M. J.; Zhang, S. B., Nondissociative adsorption of H2 molecules in light-element-doped fullerenes. *Phys. Rev. Lett.,* **2006**, *96*, 016102-016104, DOI: 10.1103/PhysRevLett.96.016102.

[34] Borch, R. F.; Millard, J. A., The mechanism of activation of 4-hydroxycyclophosphamide. *J. Med. Chem.,* **1987**, *30*, 427-431, DOI: 10.1021/jm00385a029.

[35] Vriens, B. E. P. J.; Aarts, M. J. B.; de Vries, B.; van Gastel, S. M.; Wals, J.; Smilde, T. J.; van Warmerdam, L. J. C.; de Boer, M.; van Spronsen, D. J.; Borm, G. F.; Tjan-Heijnen, V. C. G., Doxorubicin/cyclophosphamide with concurrent *versus* sequential docetaxel as neoadjuvant treatment in patients with breast cancer. *Eur. J. Cancer,* **2013**, *49*, 3102-3110, DOI:10.1016/j.ejca.2013.06.012.

[36] Frisch, M. J.; Trucks, G. W.; Schlegel, H. B.; Scuseria, G. E.; Robb, M. A.; Cheeseman, J. R.; Zakrzewski, V. G.; Montgomery, J. A.; Stratmann, R. E. J. Jr; Burant, C.; Dapprich, S.; Millam, J. M.; Daniels, A. D.; Kudin, K. N.; Strain, M. C.; Farkas, O.; Tomasi, J.; Barone V.; Cossi, M.; Cammi, R.; Mennucci, B.; Pomelli, C.; Adamo, C.; Clifford, S.; Ochterski, J.; Petersson, G. A.; Ayala, P. Y.; Cui, Q.; Morokuma, K.; Malick, D. K.; Rabuck, A. D.; Raghavachari, K.; Foresman, J. B.; Cioslowski, J.; Ortiz, J. V.; Baboul, A. G.; Stefanov, B. B.; Liu, G.; Liashenko, A.; Piskorz, P.; Komaromi, I.; Gomperts, R.; Martin, R. L.; Fox, D. J.; Keith, T.; Al-Laham, M. A.; Peng, C. Y.; Nanayakkara, A.; Challacombe, M. P.; Gill, M. W.; Johnson, B.; Chen, W.; Wong, M. W.; Andres, J. L.; Gonzalez, C.; Head-Gordon, M.; Replogle, E. S.; Pople, J. A., Gaussian 98, Revision

A9, Gaussian, Inc., Pittsburgh, PA, 1998.

[37] Bersohn, R., Nuclear electric quadrupole spectra in solids. *J. Chem. Phys.,* **1952**, *20*, 1505-1509, DOI: 10.1063/1.1700203.

[38] Pyykö, P., Spectroscopic nuclear quadrupole moments. *Mol. Phys.,* **2001**, *99*, 1617-1629, DOI: 10.1080/00268970110069010.

[39] Shariatinia, Z.; Shahidi, S., A DFT study on the physical adsorption of cyclophosphamide derivatives on the surface of fullerene C60 nanocage. *J. Mol. Graph. Model.,* **2014**, *52*, 71-81, DOI: 10.1016/j.jmgm.2014.06.001.

[40] Corbridge D. E. C., Phosphorus, An Outline of Its Chemistry, Biochemistry and Technology. 5th Ed., Elsevier, the Netherlands, 1995. DOI: 10.1021/ja965522m.

[41] Nikfar, Z.; Shariatinia, Z., Phosphate functionalized (4,4)-armchair CNTs as novel drug delivery systems for alendronate and etidronate anti-osteoporosis drugs. *J. Mol. Graph. Model.,* **2017**, *76*, 86-105, DOI: 10.1016/j.jmgm.2017.06.021.

[42] Nikfar, Z.; Shariatinia, Z. DFT computational study on the phosphate functionalized SWCNTs as efficient drug delivery systems for anti-osteoporosis zolendronate and risedronate drugs. *Physica E,* **2017**, *91*, 41-59, DOI: 10.1016/j.physe.2017.04.011.

[43] Shariatinia, Z.; Védova, C. O. D.; Erben, M. F.; Tavasolinasab, V.; Gholivand K., Synthesis, conformational and NQR analysis of phosphoric triamides containing the P(O)[N]3 skeleton. *J. Mol. Struct.,* **2012**, *1023*, 18–24, DOI: 10.1016/j.molstruc.2012.03.045.

[44] Panchuk, R. R.; Prylutska, S. V.; Chumak, V. V.; Skorokhyd, N. R.; Lehka, L. V.; Evstigneev, M. P.; Prylutskyy, Y. I.; Berger, W.; Heffeter, P.; Scharff, P.; Ritter, U.; Stoika, R. S., Application of C60 fullerene-doxorubicin complex for tumor cell treatment *in vitro* and *in vivo*. *J. Biomed. Nanotechnol.* **2015**, *11*, 1139-1152, DOI: 10.1166/jbn.2015.2058.

[45] Kojić, V.; Jakimov, D.; Bogdanović, G.; Djordjević, A. Effects of fullerenol $C_{60}(OH)_{24}$ on cytotoxicity induced by antitumor drugs on human breast carcinoma cell lines. *Mater. Sci. Forum.* **2005**, *494*, 543-548, DOI: 10.4028/www.scientific.net/

MSF.494.543.

[46] Dou, Z.; Xu, Y.; Sun, H.; Liu, Y., Synthesis of PEGylated fullerene-5-fluorouracil conjugates to enhance the antitumor effect of 5-fluorouracil. *Nanoscale.* **2012**, *4*, 4624-30, DOI: 10.1039/ c2nr30380a.

[47] Joshi, M.; Kumar, P.; Kumar, R.; Sharma, G.; Singh, B.; Katare, O. P.; Raza, K., Aminated carbon-based "cargo vehicles" for improved delivery of methotrexate to breast cancer cells. *Mater. Sci. Eng. C* **2017**, *75*, 1376-1388, DOI: 10.1016/ j.msec.2017.03.057.

[48] Misra, C.; Thotakura, N.; Kumar, R.; Singh, B.; Sharma, G.; Katare, O. P.; Raza, K., Improved cellular uptake, enhanced efficacy and promising pharmacokinetic profile of docetaxel employing glycine-tethered C60-fullerenes. *Mater. Sci. Eng. C* **2017**, *76*, 501-508, DOI:10.1016/j.msec.2017.03.073.

[49] Lapin, N. A.; Krzykawska-Serda, M.; Dilliard, S.; Mackeyev, Y.; Serda, M.; Wilson, L. J.; Curley, S. A.; Corr, S. J., The effects of non-invasive radiofrequency electric field hyperthermia on biotransport and biodistribution of fluorescent [60] fullerene derivative in a murine orthotopic model of breast adenocarcinoma. *J. Control. Release* **2017**, *260*, 92-99, DOI: 10.1016/j.jconrel.2017.05.022.